FULL PAPER

Multimodal microscopy distinguishes extracellular aggregation and cellular uptake of single walled carbon nanohorns

Stephen J. Devereux,[a] Shane Cheung,[b] Harrison C. Daly,[b] Donal F. O'Shea*[b] and Susan J. Quinn*[a]

Abstract: The low toxicity, high surface area and ease of functionalisation of carbon nanohorns (CNH) makes them attractive systems for cellular imaging, diagnostics and therapeutics. However, challenges remain for the biomedical translation of these and other nanomaterials. A significant task is tuning the surface chemistry to achieve optimal cellular interactions. Herein, we combine real-time fluorescent imaging of nanoparticle cellular uptake and real-time differential interference contrast (DIC) imaging of extracellular media to monitor (a) nanoparticle/nanoparticle and (b) nanoparticle/cell interactions for CNHs covalently modified with an OFF/ON near-infrared dye whose fluorescence is switched off in extracellular environments and triggered upon cellular internalisation. CHN samples modified with different loadings of the hydrophobic dye are taken as a simple model of drug loaded nanoparticle systems. The punctate fluorescence suggests the CNHs are delivered to lysosomes and other vesicles of the endocytic pathway. DIC imaging highlights the competition which exists for many particle types, between extracellular aggregation and cellular internalization, the efficiency of which would be dependent upon the amount of fluorophore loading. The results of this study illustrate how complementary real-time imaging methods together with physicochemical characterisation can be used to address the challenges involved in optimising nanoparticle/cell interactions for biomedical applications.

Introduction

Developing nanomaterials for cellular imaging and drug delivery is an active area of investigation towards the advancement of diagnostics and therapeutic procedures.[1-5] Numerous studies have shown nanoparticle based systems to possess key advantages over their molecular counterparts.[6, 7] Of these materials, carbon nanomaterials are among the most broadly discussed, researched and applied nanomaterials to date.[8-10] The carbon nanomaterial family constitutes a wide range of materials, which includes, carbon nanotubes, graphene, carbon nano-onions, carbon nanohorns, carbon nanodiamond and carbon dots. The chemical and optical properties of these structurally diverse materials combined with the biocompatibility of carbon has led to significant interest in their biomedical application for imaging,[11] sensing,[12] and drug delivery.[13-14]

Of the carbon nanomaterials noted above carbon nanohorns (CNH) are attractive candidates for cellular applications due to their high surface area, ease of functionalisation and low toxicity.[15, 16, 17] These nanomaterials comprise of sp^2 conical shaped postulates, with diameters of 2–5 nm and lengths of 40–50 nm, assembled into robust bud-like spherical aggregates with a diameter of between 80 and 100 nm.[18] The low toxicity revealed by in vivo and in vitro toxicological studies is linked to their metal-free synthesis.[19-21] The suitability of CNHs for in vivo studies has been further demonstrated by biodistribution studies which showed no obvious toxicologic lesions during the experiments.[22, 23] Examples of CNH delivery systems include delivery of anticancer agents,[24] controlled release of drugs,[25] and phthalocyanine hybrids for dual-modality photothermal and photodynamic therapy.[26] The biodegradation of transport materials is an important consideration when designing suitable imaging and drug delivery agents. Recently, the susceptibility of oxidised CNHs (o-CNH) to enzymatic degradation was explored, in which 60% of oxidised CNHs were degraded within 24 h in the presence of the myeloperoxidase enzyme, present in white blood cells.[27] Furthermore, some evidence suggests that appropriately functionalised CNHs can lead to activation of the immune system which may be exploited in therapies.[28, 29]

We are interested in developing CNH based cellular probes for imaging, diagnostics and therapeutics. However, challenges remain for the biomedical translation of these and other nanomaterials.[30-34] A crucial factor in realising the potential of these materials as cellular probes and delivery agents is ensuring their effective cellular uptake. This necessitates the tuning of the physical properties governing nanoscale interactions to minimize aggregation and thus allow optimal performance.[35, 36] Preparation of nanomaterials optimised for biological systems also provides access to extracellular delivery agents. However, this requires understanding of the influence of surface functionalisation, on the colloidal stability in biological media for each nanoparticle system.[34]

CNHs are intrinsically non-luminescent and therefore fluorescence based imaging of their cellular uptake has been limited and requires surface functionalisation.[37] The fluorophore immobilization on nanoparticle surfaces can yield significant photophysical benefits and is being increasingly investigated for roles in nanomedicine, nanobiotechnology and fluorescence imaging.[38-40] The surface modification can also modulate inflammatory cell recruitment of carbon nanoparticles.[41] In the present system a near-infrared boron azadipyrromethene (NIR-AZA) dye **1** was chosen as the fluorophore label (Scheme 1). This class of dye has excellent photophysical characteristics in the

[a] S. Devereux, Dr. S.Quinn
School of Chemistry
University College Dublin
Belfield, Dublin 4, Ireland
Email: susan.quinn@ucd.ie
[b] S. Cheung, H. Daly, Prof D. O'Shea
Department of Chemistry
RCSI,
123 St Stephen's Green, Dublin 2, Ireland
Email: donalfoshea@rcsi.ie

Supporting information for this article is given via a link at the end of the document

near-infrared spectral region such as tunable emission maxima between 675 and 800 nm, exceptional photostability and high quantum yields.[42] These properties have made them attractive candidates for both in vitro live cell imaging and in vivo imaging, with potential for clinical applications in fluorescence guided surgery.[43-46] The covalent attachment of this fluorophore to non-luminescent polystyrene nanoparticles was previously shown to yield a robust system whose emission was triggered by cellular uptake.[47] The OFF/ON behaviour of the dye allowed monitoring of the cellular uptake (a) in real time and (b) in the absence of background emission due to extracellular fluorophore-labelled nanoparticles.

As noted previously the colloidal stability of nanoparticles is an important consideration in the design of delivery and imaging systems. In this study we have worked to control this by preparing five covalently labelled dye-CNH samples with different dye loadings using carbodiimide chemistry[48] (Scheme 1). In this system the use of the hydrophobic fluorescent probe can be taken as a useful model for hydrophobic therapeutic molecules. The physicochemical properties of these samples were fully characterised to assess the influence of the fluorophore loading on the spectroscopic properties and colloidal stability in biological media. This information was then used to inform the cellular studies, which exploit the OFF/ON property of the dye to visualize the cellular uptake of dye modified CNH systems. In tandem, differential interference contrast (DIC) imaging has been used to report on the behaviour of extracellular non-fluorescent particles. It is important that new tools are developed to assist in the ongoing emergence of nanomaterials within biomedical fields. Monitoring the cellular uptake in this way provides a comprehensive investigation of the interplay of surface functionalisation and cellular uptake of CNHs, which is an important factor in their use as a drug delivery scaffold.

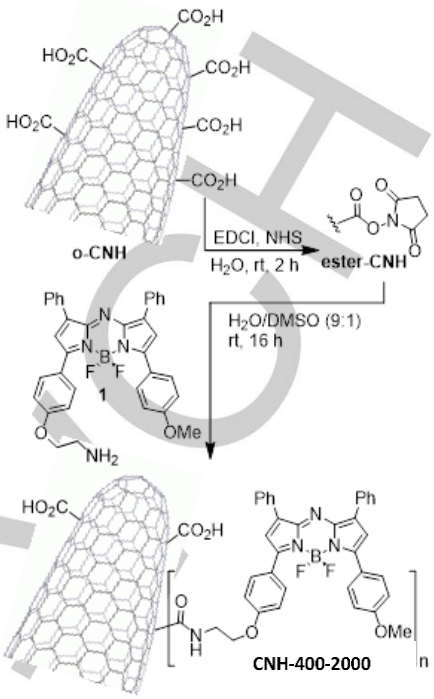

Scheme 1. CHN-400-2000 via surface functionalisation of CNHs with NIR-AZA fluorophore **1**

Results and Discussion

Preparation of NIR-fluorophore covalently labelled CNHs

Covalent linkage of the NIR-AZA fluorophore **1** to CNHs was achieved through amide bond formation using activated ester/amine coupling chemistry, which has proven successful in surface modification of other materials, see Scheme 1. In the first step, water soluble surface carboxylated o-CNH (Figure S1) were prepared by refluxing pristine CNHs in nitric acid solution for 2 h, which resulted in the creation of surface carboxylic groups whose presence was confirmed by FTIR (Figure S2).[49] The characteristic peaks of the o-CNH are ascribed to the stretching modes of O-H (2668 cm^{-1}), C=O (1788 cm^{-1}), C=C (1523 cm^{-1}) and C−O−C (at 1158 and 1030 cm^{-1}). The surface carboxylic acid groups were converted to their corresponding activated esters CNH-ester by reaction with N-hydroxysuccinimide (NHS) and 1-ethyl-3-(3-dimethylaminopropyl)carbodiimide (EDCI) at rt (Scheme 1).

Upon formation of an ester, vibrational bands at 1180 cm^{-1} and 1540 cm^{-1} were observed. These bands can be attributed to the C−O stretch and C−H stretch of an ester respectively providing further verification for the formation of an activated ester (Figure S2). Additionally, zeta potential measurements show the change in surface charge upon ester formation (Figure S3b, Table S1). These activated o-CNHs were then reacted with different stoichiometric amounts of fluorophore **1** to yield a family of NIR-AZA-CNH samples **CNH-400-2000** on the mg scale. **CNH-400-2000** samples were purified by repeated washing by centrifugation in ethanol which removed all unreacted fluorophore.

Dye loadings of 1:25 to 5:25 wgt-1/wgt-CNH (see SI Methods) were determined using a molecular weight for the CNH cluster of 5.9×10^6 g/mol. This molecular weight value was estimated from the information on the atomic composition previously obtained by neutron scattering studies.[50] The approximate loading of fluorophore molecules at each CNH particle was estimated to be in the range of 400 to 2000 molecules (Table 1).

Characterization of NIR-AZA labelled CNHs

Zeta potential measurements provide a useful probe of nanoparticle surface functional group transformations (Table S2).[51] In the case of samples **CNH-400-2000** the zeta potential (mV) was found to become progressively less negative with increased fluorophore functionalisation (Figure 1a). Dynamic light scattering (DLS) measurements revealed a negligible increase in the hydrodynamic size of o-CNHs upon functionalisation with **1**, with an average particle size of ~165 ± 70 nm (Figure S4a). Similar trends in the DLS measurements were observed in the presence of MeOH:Toluene (Figure S4b, Table S2).

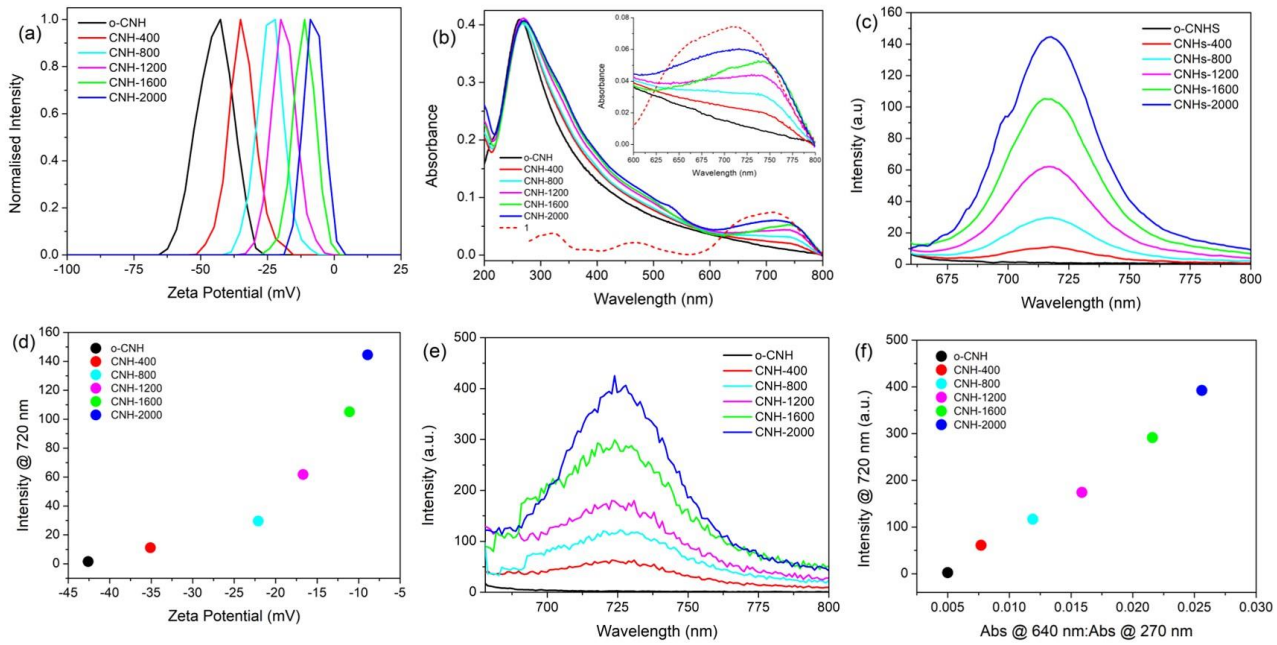

Figure 1. Characterization of **CNH-400-2000**. (a) Zeta potential measurements of functionalised CNH systems recorded in aqueous solution at pH 7.2, 25 °C. (b) UV-Vis-NIR spectra of fluorophore 1 and functionalized CNH systems in aqueous solution at pH 7.2, 25 °C. (c) Emission spectra of the CNH samples, obtained in MeOH: toluene (55:45) λ_{ex} = 640 nm. (d) Correlation of the zeta potential and emission properties of the CNHs. o-CHN (black); **CNH-400** (red); **CNH-800** (cyan); **CNH-1200** (magenta); **CNH-1600** (green); **CNH-2000** (blue). (e) Emission spectra of the o-CHN and **CNH-400-2000** in 1 mM Tx-100 (λ_{ex} = 640 nm). (f) maximum emission intensity @ 720 nm as a function of the amount of surface bound **1** expressed ratio of NIR-UV absorbance in 1 mM Tx-100 (λ_{ex} = 640 nm).

The presence of fluorophore **1** at the CNH surface was readily monitored by ultraviolet-visible-near infrared (UV-Vis-NIR) absorption spectroscopy, which showed the appearance of a band at 740 nm arising from the extended π-conjugation of the azadipyrromethene unit (Figure S5). The relative absorption of this band, compared to the absorption of the CNHs at 270 nm, was found to increase from **CNH-400** to **CNH-2000** (Figure 1b). A good correlation was observed between the increase in the absorbance of surface labelled fluorophore and of surface loading and the change in the zeta potential value (Table 1). These results show only a small change in the data between samples **CNH-1600** and **CNH-2000**, indicating that between high and maximum loading has been achieved for these samples.

As the unmodified CNHs are non-fluorescent we next considered the emission properties of **CNH400-2000** in aqueous and organic solvents. The fluorophore labelled **CNH400-2000** samples show no emission when excited at 640 nm in aqueous solution (Figure S6). Dispersion in organic solvents toluene/methanol revealed the CNH samples to be emissive with a fluorescence wavelength of maximum emission (λ_{max}) at 720 nm (Figure 1c), which is similar to that previously observed for the fluorophore alone (Figure S7). This shows that in organic solvents systems the emission properties of the fluorophore are independent of the CNH to which it is covalently bound and importantly the emission intensity was found to increase with increased levels of functionalisation with **1**, (Figure 1c, d). The fluorescence lifetime of **1** and **CNH-2000** in MeOH:Toluene (55:45) were found to be very similar, 2.77 ± 0.01 ns and 2.55 ± 0.01 ns, respectively (Table S3). Furthermore, the fluorescent lifetime found to be independent of the degree of functionalisation with similar values observed for **CNH-400** and **CNH-1200**. The quenching observed in aqueous solution is attributed to the relatively hydrophobic nature of the chosen fluorophore **1**, which results in self-quenching

Table 1. Characterisation of functionalised samples **CNH-400-2000**

Sample	o-CNH	CNH-400	CNH-800	CNH-1200	CNH-1600	CNH-2000
1 (μg): CNH(μg)	-	1:25	2:25	3:25	4:25	5:25
Loading 1:CNH[a]	-	400:1	800:1	1200:1	1600:1	2000:1
CNH $_{270nm}$:1$_{740\ nm}$	-	19.9	13.1	9.4	7.7	7.1
Size (DLS, nm)	-	161 ± 82	162 ± 60	166 ± 81	163 ± 59	167 ± 77
Zeta Potential (mV)	– 43 ± 4	– 35 ± 5	– 24 ± 4	– 17 ± 5	– 11 ± 4	– 9 ± 3

[a] Based on estimated CNH mass of 6 × 10^6 g/mol

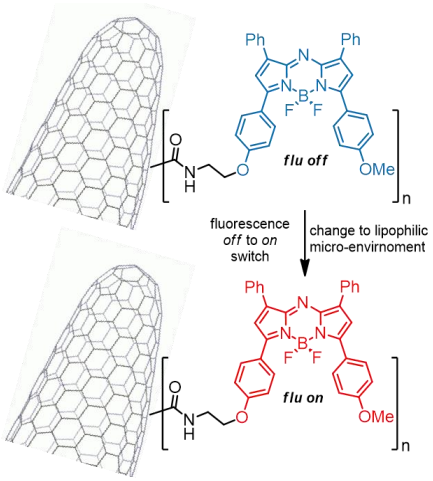

Figure 2. Basis of off to on fluorescent switch. Change in lipophilic microenvironment can be induced in aqueous solution by addition of surfactant or upon cellular uptake.[47]

and aqueous solvent quenching of the excited state (Figure S7b). This is supported by the observed shift in the absorption maximum in organic solvent (Figure S7a). The successful observation of this solvent dependent switching behaviour led us to consider the behaviour in a micelle containing solution which encountered when drugs interact with the cell membrane. Encouragingly, in the presence of a 1 mM concentration of can be considered a model for the lipophilic environment surfactant Triton-X100 solution, which is above its CMC value of 0.5 mM,[52] the fluorescence was switched ON (Figure 1e). The aqueous fluorescence lifetime of CNH-2000 in the presence of 3mM TX-100 (three times the CMC) was found to be 2.87 ± 0.01 ns, which is similar to the lifetime of the recorded in MeOH:toluene (55:45), Figure S8. DLS measurements for the CNH400-2000 sample in the presence of 3mM TX-100 showed ~20% increase in size. This is consistent with encapsulation of individual CNHs, see Figure S9 and Table S4.

The emission differences from the OFF to ON states as described by fluorescence enhancement factors (FEF) were high for each sample and reflected the level of fluorophore loading (Figure 1f). A summary of the properties for the CNH samples are given in (Table 1). The enhancement of emission in the presence of the micelle is attributed to its interaction with the particle surface and fluorophore which altered the local microenvironment of the fluorophore to being more lipophilic in nature (Figure 2).

Colloidal stability of CNH400-2000

There is significant interest in the role of the nanoparticle surface properties on their cellular uptake and ultimate destination [34-35, 53,54] A key question lies around the factors that influence non-specific protein interactions or nanoparticle fouling, which is observed under conditions of highly negative and positive charged particles.[55,56] The surface charge of nanoparticles is implicitly linked to the colloidal stability of the sample. Thus, an important consideration when preparing nanoparticle samples is their colloidal stability to the high ionic strength environment of biological buffers and cell media.[58] The resistance to aggregation under these physiological conditions is expected to be directly related to the efficacy of the nanomedicine. Figure 1d clearly shows that in these systems the enhanced luminescence associated with greater surface functionality comes at a cost to colloidal stability, as reflected in the zeta potential. The trade-off between these two factors was investigated by studying the

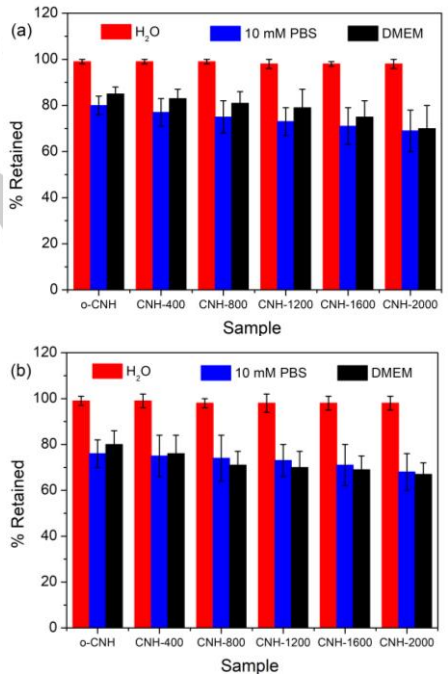

Figure 3. Summary of the colloidal stability of samples o-CHN and **CNH-400-2000** monitored by UV-Vis absorption at 268 nm showing the percentage of o-CNH and functionalized systems retained in solution after 2 h in H_2O, 10 mM PBS and DMEM at (a) 22 °C and (b) 37 °C.

Table 2. Percentage retained in solution of o-CNH and **CNH-400-2000** in H_2O, 10 mM PBS and DMEM @ 37 °C

Environment	o-CNH	CNH-400	CNH-800	CNH-1200	CNH-1600	CNH-2000
H_2O	99 ± 1	99 ± 1	98 ± 1	98 ± 2	98 ± 1	98 ± 2
PBS	76 ± 4	75 ± 6	74 ± 7	73 ± 6	71 ± 8	68 ± 9
DMEM	80 ± 3	74 ± 4	71 ± 5	70 ± 8	69 ± 7	67 ± 10

colloidal stability of **CNH-400-2000** and the parent o-CNH in (i) H_2O (ii) PBS buffer and (iii) DMEM (Dulbecco's Modified Eagle's medium). These experiments were performed by in-situ measurement of the UV-vis-NIR spectrum as a function of time at the same CNH concentrations applied in the cell studies (10 µg/mL), see Figure S10. A negligible shift in absorbance at 268 nm was observed for the stability studies performed in H_2O and 10 mM PBS, while a small 2 nm shift (Figure S10, Table S5) was observed for DMEM. Monitoring of the CNH band at 268 nm revealed excellent stability for o-CNH and **CNH-400-2000** in water (see Figure S11a). In contrast, when the samples are incubated in PBS and DMEM the absorption was found to decrease due to partial aggregation of the CNH samples leading to sedimentation. Moderate loss of sample was observed for samples **CNH-400-1200** (avg-25%) in PBS but measurably greater loss of ~30% was observed for the highly loaded samples **CNH-1600** and **CNH-2000**, (Figure 3a and Figure S11b). A slightly improved stability was observed in the presence of the DMEM with samples **CNH-400-1200** and **CNH-1600-2000** showing losses of 19% and 27% respectively (Table S6). When the measurements were repeated at 37 °C (that of cell incubation) a moderate increase in the degree of instability was observed in the presence of 10 mM PBS and DMEM, see Figure 3b, Figure S12, Table 2 and Table S7. In general, a significant amount of material was retained in the solution. The time dependent stability of the o-CNH and **CNH-400-2000** in physiological conditions (10 mM PBS, pH 7.4) and cell culture media DMEM give a truer indication of the performance of the systems in a more complex, in vivo environment compared to that of an aqueous one (Figure S13). Comparable colloidal stability studies in PBS and DMEM show the challenges that may be faced by the discrete nanoparticles when attempting to traverse a cell membrane and become internalized. These environments also show the impact of varying degrees of surface modification with fluorophore **1**. Next, a fluorescence imaging study of three CNH constructs with HeLa cells was carried to gain insight into particle cell interactions, efficiency of cellular uptake of particles and the ability of the engineered particles to elicit off to on fluorescence response upon uptake.

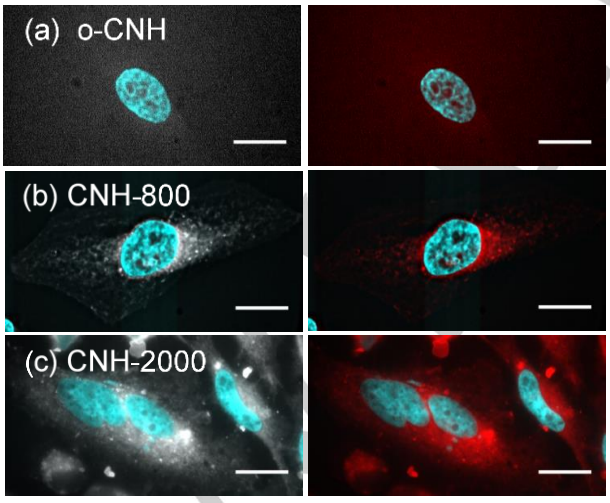

Figure 4. HeLa-Kyoto cells in DMEM were incubated with (a) o-CNH (b) **CNH-800** and (c) **CNH-2000** at 10 µg/mL concentration for 120 min, washed with PBS, fixed and nuclei stained blue with DAPI. Same image is shown with fluorescence in red (right) and white (for clarity). Scale bar = 10 µm.

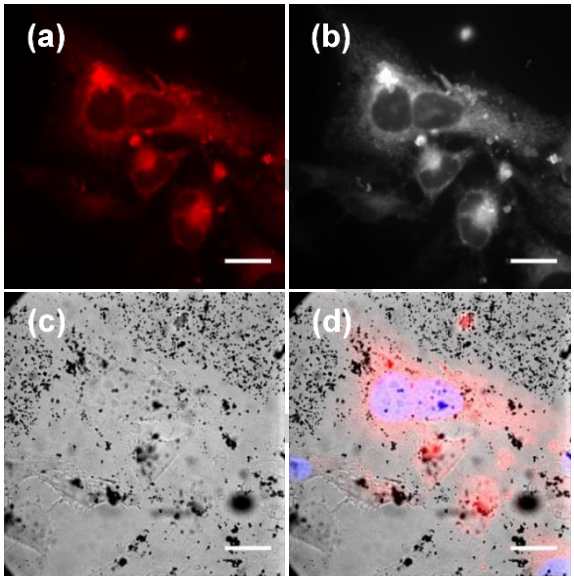

Figure 5. HeLa-Kyoto cells in DMEM were incubated with **CNH-2000** at 10 µg/mL concentration for 120 min, washed with PBS, fixed and nuclei stained blue with DAPI. (a) Fluorescence in NIR channel. (b) Identical image in black and white for clarity. (c) DIC image (d) Overlay of NIR and blue fluorescence with DIC images. Scale bar = 10 µm.

Cells which were incubated in DMEM and were treated with 10 µg/mL concentration of o-CNH, **CNH-800** and **CNH-2000** for 120 min following which the cells were washed, fixed using formaldehyde and nuclei stained using DAPI. As expected the o-CNH control showed no fluorescence whereas encouragingly both **CNH-800** and **CNH-2000** showed fluorescence indicative of cellular uptake (Figure 4). Z-Stack imaging of cells confirmed that the fluorescence was from within the cellular cytosol indicating that the particles had been efficiently internalised, and the fluorescence switched on (see movie M1 in SI). The punctate fluorescence staining pattern is indicative of uptake via endocytosis and localization within intracellular trafficking organelles. In agreement with the rapid endocytosis that was previously observed for negatively charged fluorescein labelled polystyrene nanoparticles.[56] Revealingly, when cells incubated with **CNH-2000** were viewed using differential interference contrast (DIC) imaging, the presence of non-fluorescent particles in the extra cellular media (not removed by washing prior to fixing) could be seen, see Figure 5. These were not observable with fluorescence imaging (Figure 5), or before the addition of **CNH-2000** (Figure S14). As the images reveal particle sizes larger than that of discrete nanoparticles this is taken to indicate that extracellular particle aggregation was also occurring. The formation of these larger aggregate diameters is expected to inhibit cellular uptake. This highlights the competition,

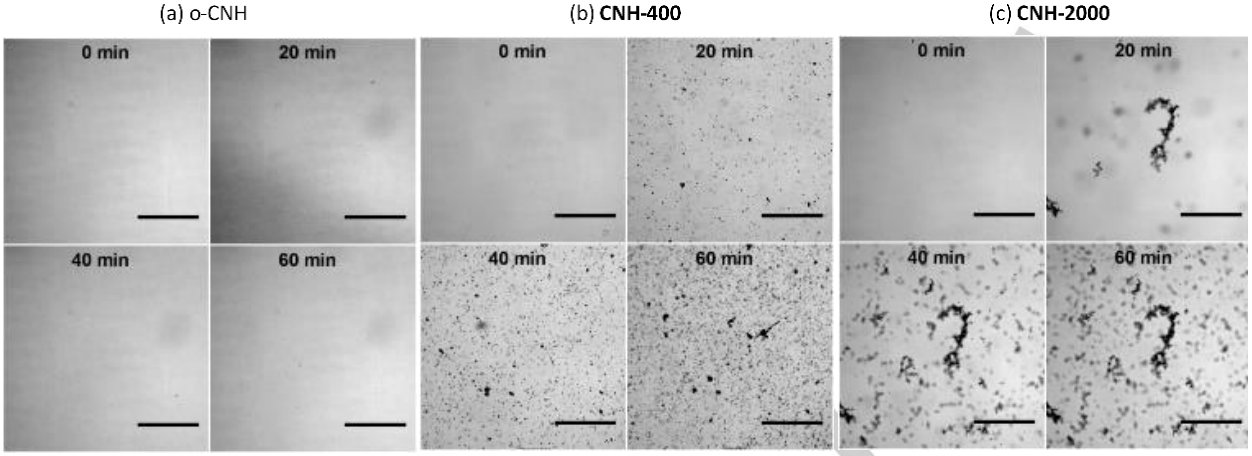

Figure 6. Continuous DIC imaging of (a) o-CNH (left), (b) **CHN-800** (middle), (c) **CNH-2000** (right) at 10 µg/mL concentration following addition to DMEM at 0, 20, 40 and 60 min. Scale bar = 10 µm.

which exists for many particle types, between extracellular aggregation and cellular internalisation, the efficiency of which would be dependent upon the amount of particle loading. The presence of aggregated nanocarbon material is commonly observed in the bright field microscopy images.[24, 48] However, the corresponding bight field movie recordings or time series confocal images that provides information on the formation of these aggregates, is rarely reported. It should be noted that while fixation may perturb intracellular location of the nanoparticles the function of the images presented is primarily to distinguish the material inside and outside the cell, which is not affected by fixation.

To gain insight into particle aggregation under imaging conditions and relate this to cellular uptake a qualitative investigation of the manner and timeframe for aggregation in cellular media without cells was carried out. This was achieved by adding the three particle types at the concentration used for imaging to cellular media with continuous DIC imaging of the media for 60 min. The compiled movies from individual time frames showed that aggregates could be seen to grow in within 20 min for **CNH-800** and **CNH-2000** and that the quantity of aggregates increased over the 60 min time period (Figure 6b, c and see movie M2, M3 in SI). In contrast, the solution o-CNH particles remained free of aggregates (Figure 6a, see move M4 in SI). This was consistent with the quantitative UV-Vis stability data, which showed that aggregation rate was dependent upon surface loading of fluorophore with **CNH-2000** aggregating more than **CNH-800**. (An important point to note is that this aggregation is not a cellular induced process but rather a particle surface controlled phenomenon which competes with cellular uptake of the non- aggregated CNHs). This real-time visualization of particle aggregation underscores the limitation of using individual time point fluorescence images alone when investigating particle/cell interactions and uptake.

As such, continuous live cell imaging, in which the cells and aggregated particles could be viewed simultaneously, utilising fluorescence and DIC microscopy was next investigated. **CNH-800** particles were chosen for this study as they showed a balance between aggregation and uptake that could be captured in a 60 min time frame allowing us to capture the internalisation of **CNH-800** with resulting switching ON of the fluorophore emission while also observing competing extracellular non-fluorescent aggregate formation. Figure 7a shows six individual time points over the 1 h time-period for an individual cell showing efficient internalisation of particles with concomitant tuning ON of the fluorescence (see movie M5 in SI). This rate of uptake indicates that there is no significant barrier to **CNH-800** particles internalisation and that the rate of

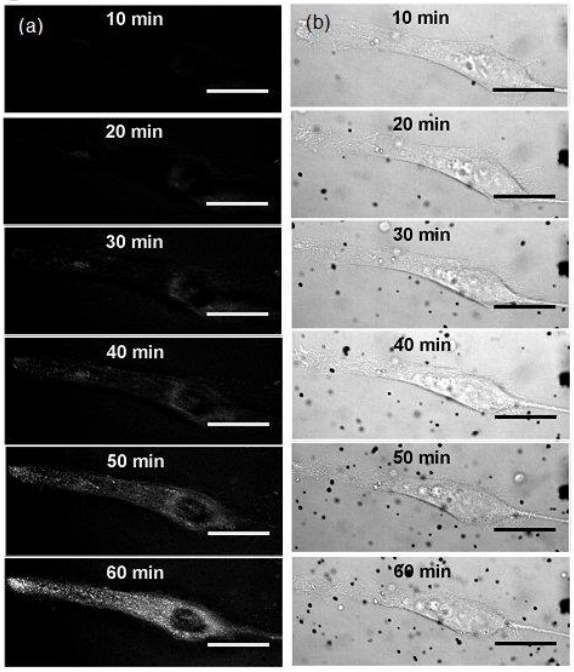

Figure 7. Real-time fluorescence and DIC imaging. **CNH-800** (10 µg/mL) were added to HeLa-Kyoto cells in DMEM and (a) NIR fluorescence and (b) DIC images acquired every 10 min for 60 min. Scale bar = 10 µm

internalisation can effectively complete with the rate of self-aggregation. Figure 7b shows the same cell imaged simultaneously in DIC in which the growth of **CNH-800** particle aggregates external to the cell body increases over the same time period (see movie M6 in SI).

Taken together the fluorescence and DIC images showed tandem processes of particle internalisation (with resulting fluorescence switching on) and aggregation over the 60 min time period. The observed aggregates appeared to be exclusively extracellular and are too big for cellular uptake while the cell cytosol remains free of aggregates indicating that once internalized particles remain relatively non-aggregated. The use of real-time simultaneous NIR-fluorescence and DIC imaging in live cells allows a more comprehensive picture of the fate of all the particles in this complex setting. Both techniques reveal an absence of nanoparticle clustering at the plasma membrane, which is characteristic of small (3-10 nm) nanoparticles.[56] Instead there seems to be a direct uptake, of the kind that has previously been attributed to a clathrin-mediated uptake.[57]

An additional key advantage lies in the fluorescence responsive nature of the surface engineered **CNH-800** which are not fluorescent in extracellular media, only establishing a fluorescence output upon cellular uptake. This permits continuous real-time imaging to be achieved as there is little background fluorescence. Illustration of this is shown in Figure 8 in which the mean intracellular fluorescence intensity over time is plotted against an extracellular region of comparable size. Graphing the change in fluorescence intensities over time show a clear accumulation and turning on of the particles within the cytosol over the 60 min time period (red trace) with negligible signal from the extracellular media (blue trace).

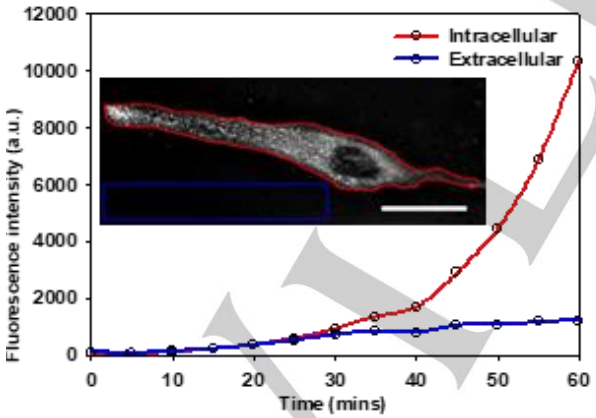

Figure 8. A region of interest (ROI) encompassing the whole cell (red line) and an extracellular region of comparable area was selected. The mean fluorescence for each ROI was measured for each 5 min time point using Image J from 0-60 min. Scale bar = 10 µm

Conclusions

We demonstrate the robust synthesis of surface modified carbon nanohorns with a varying degree of loading of NIR hydrophobic fluorophore, resulting in a highly efficient fluorescence quenching in aqueous media defining a particle's off state. Particle fluorescence can be established upon dispersion in an organic environment and in aqueous media in response to a surfactant, due to change in lipophilicity of the microenvironment. The intensity of this off on fluorescence responsive behaviour is dependent on the degree of fluorophore functionalisation and in turn impacts on the colloidal stability of the nanoparticle, wherein it was determined that as the loading of the hydrophobic fluorophore increases the colloidal stability decreases.

Studies in contrasting environments such as water, PBS and biological media DMEM shows that stability is related to the degree of surface loading and the media in which the assessment is made. This off on fluorescence responsive behaviour has been extrapolated into a real time biological imaging domain in which the cellular uptake of the particles with inclusion within organelles mimics the off on switching obtained with surfactants and in the presence of an organic environment. Continuous real-time imaging of cellular uptake provided a large signal to noise ratio with minimal background fluorescence. The punctate fluorescence suggests that the CNHs are located in lysosomes or some other vesicles of the endocytic pathway.

DIC imaging highlights the competition which exists for many particle types, between extracellular aggregation and cellular internalisation, the efficiency of which would be dependent upon the amount of fluorophore loading. Taken together, this use of tandem NIR-fluorescence and DIC imaging with bio-responsive off to on fluorescent CNHs allows the visualization of complex particle/particle and particle/cell interactions in real time providing a more comprehensive view of particle performance. Importantly, this approach provides information regarding the optimal surface functionality required to offset the competition between extracellular aggregation and cellular internalisation.

Experimental Section

Carbon Nanohorn functionalization

Pristine CNH (10 mg) in 5 M nitric acid (50 mL) were heated under reflux for 2 h. The resulting suspension was centrifuged at 10,000 rpm to form a pellet of o-CNH and repeatedly washed with water (45 mL) until the supernatant was neutral. The o-CNHs were dispersed in water (10 mL) by sonication. EDCI (0.25 mol/L, 100 µL) and NHS (0.25 mol/L, 100 µL) were added to a suspension of o-CNH (0.5 mg/mL, 2.5 mL) in H_2O (2.5 mL) and the solution stirred for

2 h at 20 °C. After which the fluorophore **1** (1 mg/mL, 900 µL in DMSO) was added and stirring continued for 16 h. Particles were purified by repeated washing and centrifugation at 13,000 rpm from ethanol. **CNH-400** were then washed three times with water by centrifugation at 13,000 rpm to remove ethanol and washed pellets dispersed in H_2O (2 mL). Tunable functionalisation of **CNH-400-2000** was achieved by varying the amount of fluorophore **1** in each corresponding reaction. Known volumes (50-250 µL, incrementing by 50 µL) of fluorophore **1** (1 mg/mL, in DMSO) were added to 5 separate reaction vessels each containing a suspension of CNH-ester (0.5 mg/mL, 2.7 mL). Each reaction mixture was then stirred overnight and an identical washing procedure repeated as above.

Stability to aggregation of CNH-400-2000

The colloidal stability of the functionalised CNHs were considered in comparison with the parent o-CNHs in (i) H_2O (ii) PBS and (iii) DMEM supplemented with 10% foetal bovine serum (FBS), 1% penicillin/ streptomycin, and 1% L-glutamate. These measurements were performed in a UV-visible spectrometer by monitoring the strongly absorbing CNH band at 268 nm as a function of time under conditions of concentration that were to be applied in the cell studies (10 µg/mL).

Characterization Techniques UV-Vis

UV-visible absorption spectra were recorded at room temperature using a Cary 50 scanning spectrometer. Emission spectra were recorded using a Varian Cary Eclipse Fluorescence Spectrophotometer working in fluorescence mode. All samples were examined in a 1 cm quartz cell and were optically dilute at the excitation wavelength. Scanning Electron Microscopy (SEM) was carried out on a Zeiss Ultra Plus microscope, operating at 10 kV, using the In-lens detector. Dynamic light scattering and zeta potential measurements were carried out on a Malvern Zetasizer Nano-ZS, equipped with a 4 mW He-Ne laser operating at 632.8 nm, measurements were taken at 173°.

Fluorescence off/on switching CNH400-2000

CNH400-2000 were dispersed in a ratio of MeOH:toluene (55:45, 3 mL) or Tx-100 (1 mM. 3 mL) to a concentration of (10 µg/mL). Each suspension was sonicated for 5 min and vortexed. **CNH-400-2000** were excited at 640 nm and emission monitored at 720 nm.

Real-time imaging of CNH aggregation DMEM

DMEM was added to a well in a glass bottomed chamber slide, while retaining focus on the selected field of view an aliquot of DMEM containing o-CNH, **CNH-400** or **CNH-2000** was added to give a final concentration of 10 µg/mL. Images were immediately acquired in the bright-field channel at 3 min intervals to produce a time-lapse video.

Fixed cell imaging HeLa

HeLa Kyoto cells were seeded at a density of 1 x 104 cells/well on eight well removable chamber slide (Millipore), and allowed to proliferate for 24 h at 5.0% CO_2 and 37 °C. Cells were cultured in DMEM supplemented with 10% foetal bovine serum (FBS), 1% penicillin/ streptomycin, and 1% L-glutamate. Cells were then incubated with solutions of DMEM containing 10 µg/mL o-CNH, **CNH-800**, or **CNH-2000** for 120 min, washed with PBS and then fixed with 4.0% para-formaldehyde for 5 min. After an additional washing step, a coverslip was mounted using Vectashield mounting media containing DAPI to counterstain nuclei. Fluorescence and DIC images were acquired on an Olympus IX73 epi-fluorescent microscope fitted with an Andor iXon Ultra 888 EMCCD, using a 60x/1.42 oil PlanApo objective (Olympus). and controlled by MetaMorph (v7.8). Fluorescence illumination was provided by a Lumencor Spectra X light engine containing a solid state light source. DAPI: Excitation filter = 390 (40) nm, emission filter = 435 (48) nm. NIR: Excitation filter = 640 (14) nm. Emission filter = 705 (72) nm.

Live cell imaging HeLa

HeLa Kyoto cells were seeded at a density of 1 x 104 cells per well on a glass bottomed chamber slide (Ibidi) and allowed to proliferate for 24 h at 5.0% CO_2 and 37 °C. Cells were cultured in DMEM supplemented with 10% foetal bovine serum (FBS), 1% penicillin/streptomyosin, and 1% L-glutamate. The slide was place on the microscope stage surrounded by an incubator to maintain the temperature at 37 °C and CO_2 at 5.0%. DIC imaging was used to choose a field of view and focus on a group of cells. Cell media was removed from the well and replaced with DMEM containing 10 µg/mL **CNH-800**. Time-lapse imaging was performed by maintaining focus on cells in the chosen field of view and acquiring images every 5 min for 60 min in the NIR and DIC channels. Images were acquired on the same microscope system as described above.

Using the image processing software ImageJ a ROI encompassing a single cell, and a second extracellular ROI were manually selected. The mean grey level value in each ROI was measured at every time-point and plotted over time.

Acknowledgements

We are grateful to Prof. Kenneth Dawson, Director of the Centre for BioNano Interactions (CBNI), for access to the DLS instrumentation.

DOS gratefully acknowledges Science Foundation Ireland grant number 11/PI/1071(T) for financial support.

This work was supported by the Irish Research Council (GOIPG/2016/805, SJD) and UCD

Keywords: Labelled Carbon Nanohorns • Live cell imaging • Surface functionalisation • Nanomaterials • Aza-Boron-dipyrromethenes • NIR-AZA fluorophores

A patent application has been filed on azadipyrromethene based NIR fluorophores (PCT/EP2010/065991) in which DOS has a financial interest.

[1] S. E. McNeil, Wiley Interdiscip. Rev. Nanomedicine Nanobiotechnology, 2009, **1**, 264.
[2] T. H. Kim, S. Lee, X. Chen, *Expert Rev. Mol. Diagnostics*. 2013, **13**, 257.
[3] S. K. Murthy, *Int. J. Nanomedicine*, 2007, **2**, 129.
[4] V. Biju, *Chem. Soc. Rev*., 2014, **43**, 744.
[5] V. P. Torchilin, *Nat. Rev. Drug Discov*., 2014, **13**, 813.
[6] H. S. Choi and J. V. Frangioni, *Mol. Imaging*, 2010, **9**, 291.
[7] A. C. Anselmo, S. Mitragotri, *Bioeng. Transl. Med*., 2016, **1**, 10.
[8] P. Article*, Nat. Mater*., 2007, **6**, 183.
[9] V. Georgakilas, J. A. Perman, J. Tucek, R. Zboril, *Chem. Rev*., 2015, **115**, 4744.
[10] J. Wen, Y. Xu, H. Li, A. Lu, S. Sun, *Chem. Commun*., 2015, **51**, 11346.
[11] (a) J. Bartelmess, S. J. Quinn and S. Giordani, *Chem. Soc. Rev*., 2015, **44**, 4672; (b) M. Frasconi, R. Marotta, L. Markey, K. Flavin, V. Spampinato, G. Ceccone, L. Echegoyen, E. M. Scanlan, S. Giordani, *Chem. Eur. J.* 2015, **21**, 19071.
[12] F. R. Baptista, S. A. Belhout, S. Giordani, S. J. Quinn, *Chem. Soc. Rev*., 2015, **44**, 4433.
[13] Z. Liu, A. C. Fan, K. Rakhra, S. Sherlock, A. Goodwin, X. Chen, Q. Yang, D. W. Felsher, H. Dai, *Angew. Chemie - Int. Ed*., 2009, **48**, 7668.
[14] C. Chung, Y. K. Kim, D. Shin, S. R. Ryoo, B. H. Hong, D. H. Min, Acc. *Chem. Res*., 2013, **46**, 2211.
[15] S. Zhu and G. Xu, Nanoscale, 2010, **2**, 2538.
[16] N. Karousis, I. Suarez-Martinez, C. P. Ewels, N. Tagmatarchis, *Chem. Rev*., 2016, **116**, 4850.
[17] X. Fan, J. Tan, G. Zhang, F. Zhang, *Nanotechnology*, 2007, **18**, 195103.
[18] S. Iijima, M. Yudasaka, R. Yamada, S. Bandow, K. Suenaga, F. Kokai, K. Takahashi, *Chem. Phys. Lett*., 1999, **309**, 165.
[19] J. Miyawaki, M. Yudasaka, T. Azami, Y. Kubo, S. Iijima, *ACS Nano*, 2008, **2**, 213.
[20] M. Horie, L. K. Komaba, H. Fukui, H. Kato, S. Endoh, A. Nakamura, A. Miyauchi, J. Maru, E. Miyako, K. Fujita, Y. Hagihara, Y. Yoshida, H. Iwahashi, *Carbon N. Y*., 2013, **54**, 155.
[21] R. M. Lynch, B. H. Voy, D. F. Glass, S. M. Mahurin, B. Zhao, H. Hu, A. M. Saxton, R. L. Donnell, M. D. Cheng, *Nanotoxicology*, 2007, **1**, 157.
[22] Y. Tahara, J. Miyawaki, M. Zhang, M. Yang, I. Waga, S. Iijima, H. Irie, M. Yudasaka, *Nanotechnology*, 2011, **22**, 265106.
[23] M. Zhang, T. Yamaguchi, S. Iijima, M. Yudasaka, *Nanomedicine Nanotechnology, Biol. Med*., 2013, **9**, 657.
[24] (a) K. Ajima, M. Yudasaka, T. Murakami, A. Maigné, K. Shiba and S. Iijima, *Mol. Pharm*., 2005, **2**, 475; (b) R. Wang, H. Cui, J. Wang, N. Li, Q. Zhao, Y. Zhou, Z. Lv, W. Zhong *RSC Adv.*, 2016, **6**, 47272
[25] J. Xu, M. Yudasaka, S. Kouraba, M. Sekido, Y. Yamamoto, S. Iijima, *Chem. Phys. Lett*., 2008, **461**, 189.
[26] B. P. Jiang, L. F. Hu, X. C. Shen, S. C. Ji, Z. Shi, C. J. Liu, L. Zhang, H. Liang, *ACS Appl. Mater. Interfaces*, 2014, **6**, 18008.
[27] M. Zhang, M. Yang, C. Bussy, S. Iijima, K. Kostarelos, M. Yudasaka, *Nanoscale*, 2015, **7**, 2834.
[28] S. Lacotte, A. García, M. Décossas, W. T. Al-Jamal, S. Li, K. Kostarelos, S. Muller, M. Prato, H. Dumortier, A. Bianco, *Adv. Mater*., 2008, **20**, 2421.
[29] B. S. Zolnik, Á. González-Fernández, N. Sadrieh, M. A. Dobrovolskaia, *Endocrinology*, 2010, **151**, 458.
[30] E. Blanco, H. Shen, M. Ferrari, *Nat. Biotechnol*., 2015, **33**, 941.
[31] J. Shi, P. W. Kantoff, R. Wooster, O. C. Farokhzad, *Nat. Rev. Cancer*, 2017, **17**, 20.
[32] Y. Nakamura, A. Mochida, P. L. Choyke, H. Kobayashi, *Bioconjug. Chem*., 2016, **27**, 2225.
[33] H. Chen, W. Zhang, G. Zhu, J. Xie, X. Chen, *Nature Reviews Materials*. 2017, **2**, 17024.
[34] A. E. Nel, L. Mädler, D. Velegol, T. Xia, E. M. V. Hoek, P. Somasundaran, F. Klaessig, V. Castranova, M. Thompson, *Nat. Mater*., 2009, **8**, 543.
[35] C. Pfeiffer, C. Rehbock, D. Huhn, C. Carrillo-Carrion, D. J. de Aberasturi, V. Merk, S. Barcikowski, W. J. Parak, J. *R. Soc. Interface*, 2014, **11**, 20130931.
[36] L. A. Lane, X. Qian, A. M. Smith, S. Nie, Annu. *Rev. Phys. Chem*., 2015, **66**, 521.
[37] J. Li, Z. He, C. Guo, L. Wang, S. Xu, *J. Lumin*., 2014, **145**, 74.
[38] W. J. Stark, *Angew. Chemie - Int. Ed*., 2011, **50**, 1242.
[39] X. He, K. Wang, Z. Cheng, Wiley Interdiscip. Rev. Nanomedicine Nanobiotechnology, 2010, **2**, 349.
[40] P. Rungta, Y. P. Bandera, R. D. Roeder, Y. Li, W. S. Baldwin, D. Sharma, M. G. Sehorn, I. Luzinov, S. H. Foulger, *Macromol. Biosci*., 2011, **11**, 927.
[41] M. Yang, K. Flavin, I. Kopf, G. Radics, C. H. A. Hearnden, G. J. McManus, B. Moran, A. Villalta-Cerdas, L. A. Echegoyen, S. Giordani, E. C. Lavelle, *Small*, 2013, **9**, 4194.
[42] (a) Y. Ge, D. F. O'Shea, *Chem. Soc. Rev*., 2016, **45**, 3846; (b) S. Cheung, D.F. O'Shea, *Nat. Commun*., 2017, **8**, 1885.
[43] (a) D. Wu, S. Cheung, M. Devocelle, L.-J. Zhang, Z.-L. Chen, D. F. O'Shea, *Chem. Commun*., 2015, **51**, 16667; (b) J. Killoran, D.F. O'Shea, Chem. Commun., 2006, **14**, 1503.
[44] H. C. Daly, G. Sampedro, C. Bon, D. Wu, G. Ismail, R. A. Cahill, D. F. O'Shea, *Eur. J. Med. Chem*., 2017, **135**, 392.
[45] M. Grossi, M. Morgunova, S. Cheung, D. Scholz, E. Conroy, M. Terrile, A. Panarella, J. C. Simpson, W. M. Gallagher, D. F. O'Shea, *Nat. Commun*., 2016, **7**, 10855.
[46] (a) D. Wu, D. F. O'Shea, *Chem. Commun*., 2017, **53**, 10804. (b) M. Grossi, A. Palma, S.O. McDonnell, M.J. Hall, D.K. Rai, J. Muldoon, D.F. O'Shea, J. Org. Chem., 2012, **77**, 9304.
[47] A. Palma, L. A. Alvarez, D. Scholz, D. O. Frimannsson, M. Grossi, S. J. Quinn, D. F. O'Shea, *J. Am. Chem. Soc*., 2011, **133**, 19618.
[48] M. Zhang, M. Yudasaka, K. Ajima, J. Miyawaki, S. Iijima, *ACS Nano*, 2007, **1**, 265.
[49] G. Rotas, A. S. D. Sandanayaka, N. Tagmatarchis, T. Ichihashi, M. Yudasaka, S. Iijima, O. Ito, *J. Am. Chem. Soc*., 2008, **130**, 4725.
[50] L. Hawelek, A. Brodka, J. C. Dore, A. C. Hannon, S. Iijima, M. Yudasaka, T. Ohba, K. Kaneko, A. Burian*, J. Phys. Chem*. A, 2013, **117**, 9057.
[51] F. Thielbeer, K. Donaldson, M. Bradley, *Bioconjug. Chem*., 2011, **22**, 144.
[52] A. B. Mandal, B. U. Nair, D. Ramaswamy, *Langmuir*, 1988, **4**, 736.
[53] Y. Jiang, S. Huo, T. Mizuhara, R. Das, Y. W. Lee, S. Hou, D. F. Moyano, B. Duncan, X. J. Liang, V. M. Rotello, *ACS Nano*, 2015, **9**, 9986.
[54] J. D. Feick, N. Chukwumah, A. E. Noel, D. Velegol, *Langmuir*, 2004, **20**, 3090.
[55] M. Lundqvist, J. Stigler, G. Elia, I. Lynch, T. Cedervall, K. A. Dawson, *Proc. Natl. Acad. Sci. U. S. A*., 2008, **105**, 14265.
[56] L. Shang, K. Nienhaus, X. Jiang, L. Yang, K. Landfester, V. Mailänder, T. Simmet, G. U. Nienhaus, *Beilstein J. Nanotechnology*, 2014, **5**, 2388.
[57] X. Jiang, A. Musyanovych, C. Röcker, K. Landfester, V. Mailänder, G. U. Nienhaus, *Nanoscale*, 2011, **3**, 2028–2035
[58] S. A. Belhout, J. Y. Kim, D. T. Hinds, N. J. Owen, J. A. Coulter, S. J. Quinn, *Chem. Commun*., 2016, **52**, 14388.

Layout 1:

FULL PAPER

In-vivo behaviour of CHN samples covalently modified with different loadings of the hydrophobic dye taken as a simple model of drug loaded nanoparticle systems.

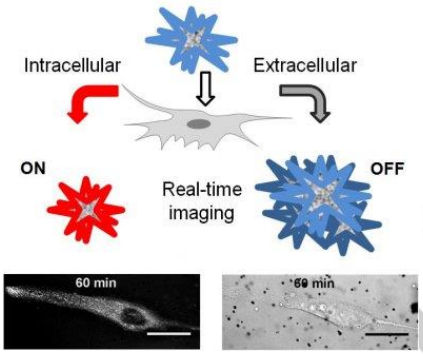

Stephen J. Devereux, Shane Cheung, Harrison C. Daly, Donal F. O'Shea and Susan J. Quinn**

Page No. – Page No.
Multimodal microscopy distinguishes extracellular aggregation and cellular uptake of single walled carbon nanohorns